SI Appendix

Structures of trehalose-6-phosphate phosphatase from pathogenic fungi reveal the mechanisms of substrate recognition and catalysis

Yi Miao[a], Jennifer L. Tenor[b], Dena L. Toffaletti[b], Erica J. Washington[a], Jiuyu Liu[c], William R. Shadrick[c], Maria A. Schumacher[a], Richard E. Lee[c], John R. Perfect[b], and Richard G. Brennan[a,1]

a. Department of Biochemistry, Duke University School of Medicine, Durham, North Carolina, 27710 USA

b. Division of Infectious Diseases, Department of Medicine, Duke University Medical Center, Durham, North Carolina, 27710 USA

c. Department of Chemical Biology and Therapeutics, St. Jude Children's Research Hospital, Memphis, Tennessee, 38105 USA

[1]To whom correspondence should be addressed: richard.brennan@duke.edu

SI Appendix Materials and Methods

Purification and crystallization of *C. albicans* Tps2 domains

The *tps2NTD* gene (residues 1-534) and *tps2PD* gene (residues 535-833 but refered to as residues 1-299 throughout this manuscript) from *C. albicans* strain SC5314 were cloned from a cDNA library into the pMCSG7 plasmid using a standard ligation-independent cloning protocol (1). Tps2NTD residue 120 was mutated to serine since CTG encodes serine in *C. albicans* (2) but leucine in *E. coli*. The pMCSG7 vector contains an N-terminal hexahistidine affinity tag followed by a TEV protease cleavage site. Tps2NTD and Tps2PD were expressed in Rosetta 2(DE3) pLysS cells (Novagen) and were induced with 0.5 mM IPTG at 15 °C. Tps2NTD and Tps2PD proteins were purified by Ni^{2+}-NTA affinity column chromatography followed by TEV protease cleavage of the His-tag. The cleaved proteins were reloaded onto the Ni^{2+}-NTA column to eliminate non-cleaved protein and TEV protease, which also contains a histidine tag. The proteins were further purified by size exclusion chromatography (SEC). To prepare single residue mutated Tps2PD, a standard site directed mutagenesis protocol was utilized (3). All mutated DNA was sequenced to assure the proper mutations were made. Each mutated Tps2PD was purified as described for the wild-type protein. *C. albicans* Tps2NTD was concentrated to 20 mg/mL and crystals were grown at 25 °C by the hanging drop-vapor diffusion method. Protein crystals appeared after one week from solutions of 1.2 M sodium citrate and 0.1 M cacodylate pH 6.5. *C. albicans* Tps2PD was concentrated to 45 mg/mL and co-crystallized with 50 mM trehalose and 50 mM beryllium fluoride. Crystals were grown at 25 °C by the hanging drop-vapor diffusion

method. Protein crystals appeared after one week from solutions of 0.2 M lithium sulphate, 0.1 M Tris pH 7.0 and 2.0 M ammonium sulphate.

Protein expression and crystallization of the Tps2PD from *C. neoformans* and *A. fumigatus*

tps2PD genes from *A. fumigatus* and *C. neoformans* were codon optimized for *E. coli* expression system (GenScript). To prepare the *C. neoformans* Tps2 D24N mutant, a standard site directed mutagenesis protocol was utilized (3). These codon-optimized genes were cloned into a pET-28b kanamycin-resistant vector using the restriction sites *NcoI* and *XhoI*. This vector contained a C-terminal un-cleavable hexahistidine affinity tag. The vectors were transformed into BL21(DE3) plysS cells (Life Technologies) and were induced with 0.5 mM IPTG at 15 °C for 16 h. Tps2PD was purified by Ni^{2+}-NTA affinity column chromatography and subsequent SEC using a Superdex S75 column (GE Healthcare). Purified Tps2PD was concentrated in Buffer (20 mM HEPES, pH 7.5, 100 mM NaCl, 5% glycerol, 5 mM $MgCl_2$, and 1 mM βME) using an Amicon Ultra concentrator (10K MWCO, Millipore). *C. neoformans* Tps2PD was concentrated to 12 mg/mL and co-crystallized with 5 mM T6P. Crystals were grown at 25 °C by hanging drop-vapor diffusion method. Protein crystals appeared after two weeks from solutions of 0.1 M $MgCl_2$, 0.1 M Tris pH 8.5, 20% PEG 400 and 10% PEG 8000. *A. fumigatus* crystals were grown at 25 °C by hanging drop-vapor diffusion method using 20 mg/mL protein. Form 1 crystals appeared after two weeks from solutions of 0.1 M sodium citrate, pH 5.5, 16% PEG 8000. Form 2 crystals appeared two weeks from solutions of

0.1 M HEPES, pH 7.0, 15% PEG 20000. Form 3 crystals appeared after two weeks from solutions of 0.1 M HEPES, pH 7.5, 12% PEG 3350.

X-ray data collection and structure determination

Intensity data for the *C. albicans* Tps2NTD crystals were collected to 2.56 Å resolution at the Advanced Photon Source (APS) using the ID-22 beamline. The Tps2NTD structure was determined by molecular replacement using Phaser (4) and the structure of OtsA, the Tps1 from *E. coli*, (PDB code: 1UQU) (5) as the search model. The intensity data for the *C. albicans* Tps2PD and selenomethionine (SeMet)-substituted Data for the Tps2PD crystals were collected to 2.0 Å and 2.12 Å resolution, respectively, at the Advanced Light Source (ALS) using beamlines 5.0.1 and 5.0.2. Experimental phases were calculated using Phenix Autosol (6) and the model was manually built in Coot (7). Intensity data for the *C. neoformans* Tps2PD crystal were collected to 2.15 Å resolution using ALS beamline 5.0.1. The structure was determined by molecular replacement using the *C. albicans* Tps2PD as a search model. Data for the *A. fumigatus* SeMet-substituted protein crystal and native crystals were collected using the APS BM-22 and ID-22 beamlines, respectively. Experimental phases were calculated using Phenix Autosol (6) and the model was manually built in Coot (7). All data were indexed and scaled using HKL2000 (8). All models were improved using multiple rounds of refinement using Phenix.refine (9) followed by model rebuilding. Selected statistics of data collection and refinement are presented in Table S2 and Table S3.

Steady-state kinetics and protein activity assay

To measure the steady-state kinetics of the *C. albicans* Tps2PD, the initial enzyme velocity was measured utilizing 3 nM Tps2PD with a gradient concentration of T6P (0.05 mM to 1.5 mM). Similarly, initial enzyme velocities of selected Tps2PD variants were measured utilizing 50 to 300 nM protein with a gradient concentration of T6P (0.05 mM to 6 mM). The assays were performed using the EnzChek Phosphate Assay Kit (Molecular Probes) and absorbance at 360 nm was measured using a SpectraMax M5 plate reader (Molecular Devices). All measurements were performed in triplicate. Data were fit using the Michaelis-Menten kinetics module as implemented in GraphPad Prism 6.

Cell survival assays and capsule induction in *C. neoformans*

Cryptococcus neoformans var. *grubii* strain H99 was used for this study. PCR based site-directed mutagenesis in combination with the In-Fusion HD cloning system was used to generate two mutated proteins: a truncated Tps2 protein (682-987) and a Tps2 protein containing a D705N mutation. Each DNA construct was transformed into a *tps2*Δ mutant strain by biolistic transformation (10). To examine cells for capsule production, a capsule-inducing medium was used as described with minor changes (11). Briefly, a single colony of yeast was inoculated into 5 mL YPD broth and grown at 30 ˚C overnight on a shaking incubator (225 rpm). Cells were harvested by centrifugation at 3000 rpm for 3 minutes and washed twice with 10 mL PBS. The cell pellet was resuspended in 5 mL diluted Sabouraud (1/1) in MOPS buffer pH 7.3. The cells were grown overnight under the same conditions and stained the next day with India Ink for

visualization of capsule. A Zeiss Axio Imager A1 fluorescence microscope equipped with an AxioCam MRM digital camera was used to capture differential interference contrast (DIC) images under oil immersion at 63X magnification. Images were acquired and analyzed by ZEN software (Zeiss).

SI Appendix Figures

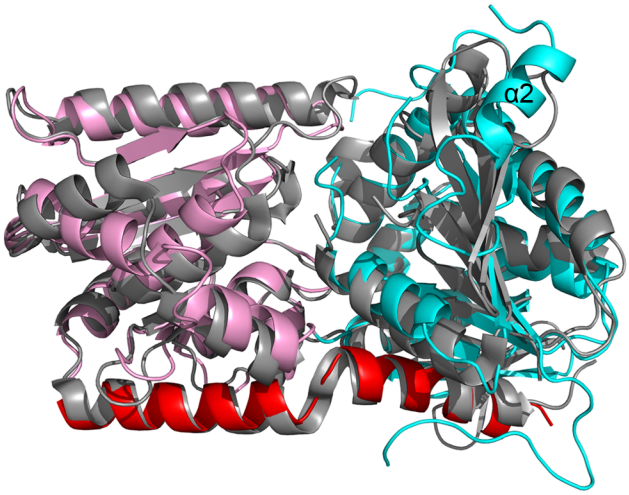

Figure S1. Superposition of *C. albicans* Tps2NTD and *E. coli* OtsA.

Superposition of Tps2NTD and *E. coli* OtsA, the latter of which is colored grey. Note the significant difference of the N-terminal Rossmann fold domains (cyan on grey).

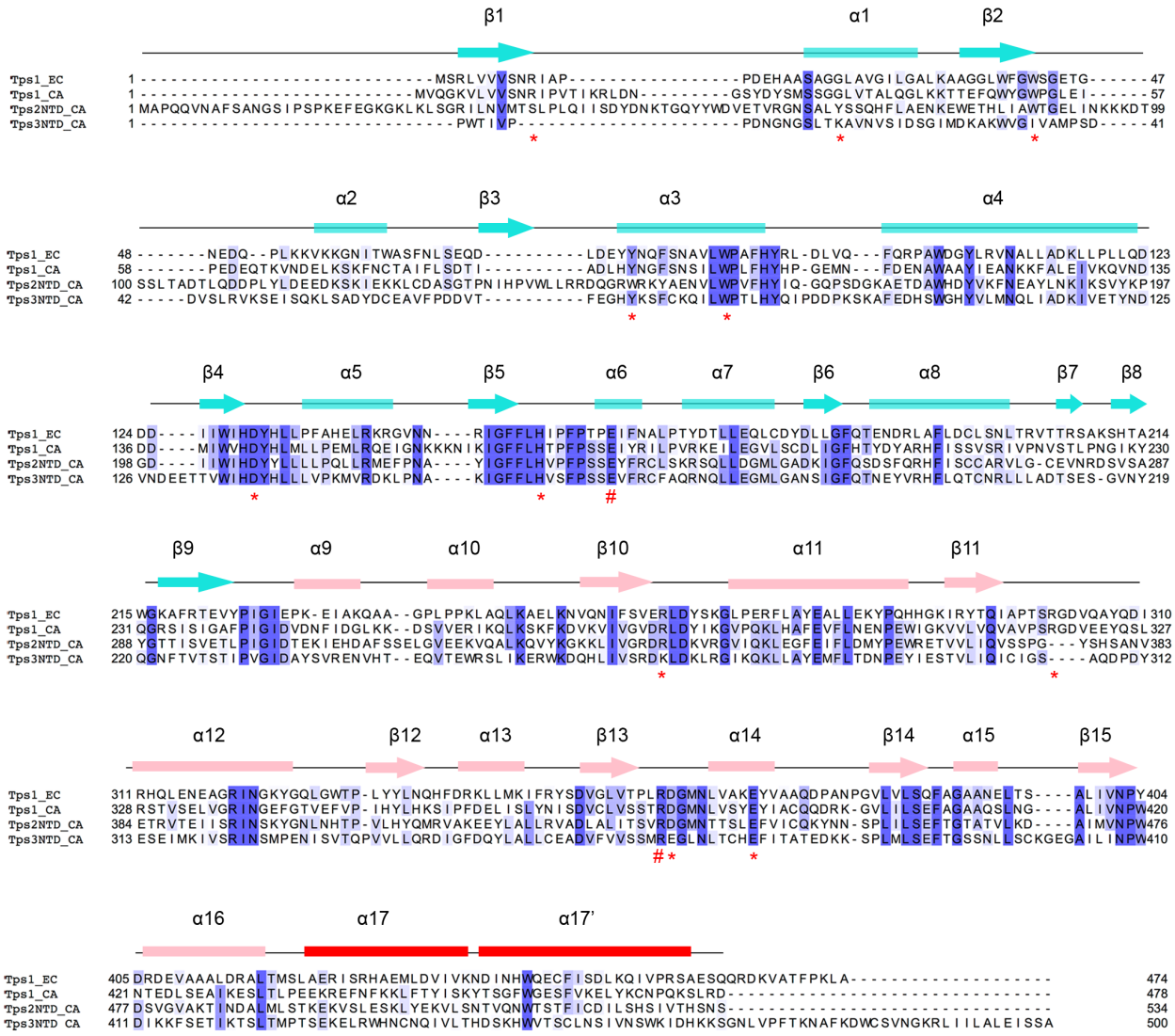

Figure S2. Sequence alignment of *C. albicans* Tps2NTD.

Primary sequences of *C. albicans* Tps2NTD (Q5AI14), *E. coli* OtsA (labelled as Tps1_EC) (P31677), *C. albicans* Tps1 (Q92410) and *C. albicans* Tps3NTD (residues 234-833) were aligned. Identical and highly conserved residues are shaded in the figure. Red asterisks denote teh catalytic residues of *E. coli* OtsA. The red pound signs point out two key residues involved in *E. coli* OtsA tetramer formation.

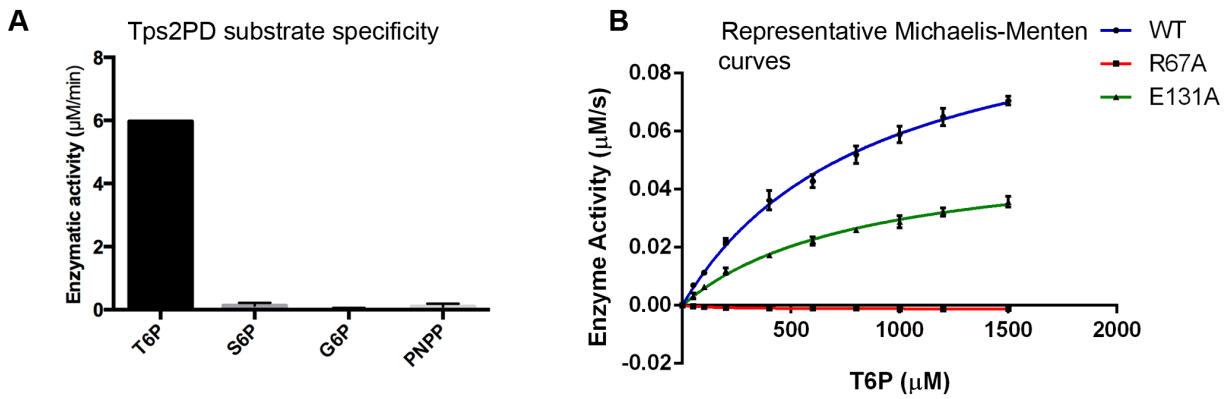

Figure S3. *C. albicans* Tps2PD activity assays.

(**A**) Tps2PD selectivity for different substrates. The error bars on the graph represent the S.E. of three independent measurements. (**B**) Representative Michaelis-Menten kinetic curves of Tps2PD WT and selected variants. Protein concentrations of Tps2PD WT and variants (R67A and E131A) are 3 nM and 50 nM, respectively. The statistical data were analyzed and figures generated using GraphPad Prism6. The error bars represent the standard deviation (S.D.) of three independent measurements.

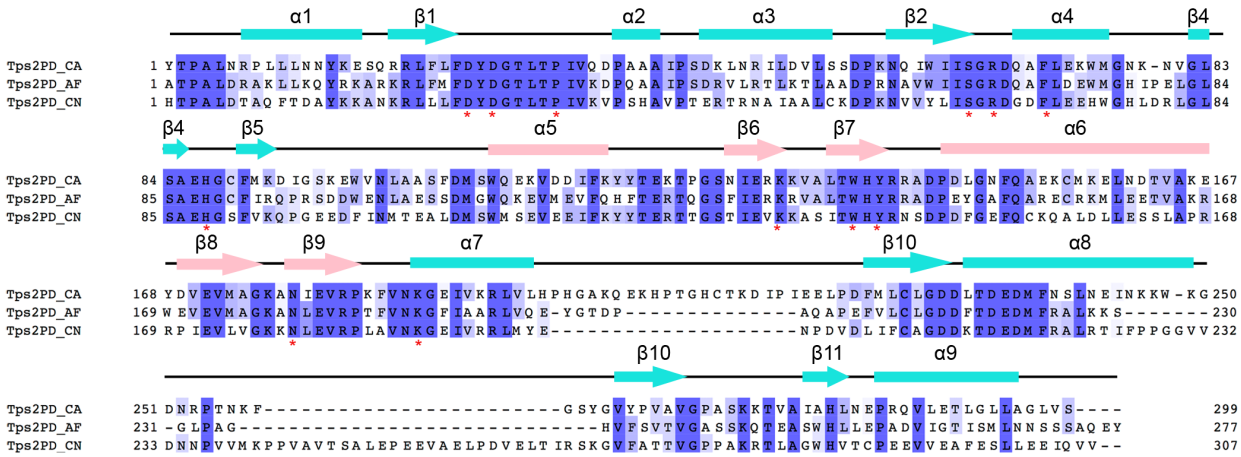

Figure S4. Sequence alignment of Tps2PD.

Primary sequences of *C. albicans* Tps2PD (Q5AI14 residues 535-833), *A. fumigatus* Tps2PD (A0A084BMG6 residues 673-949) and *C. neoformans* Tps2PD (Q059G6 residues 681-987) are aligned. Identical and highly conserved residues are shaded and residues involved in catalysis and substrate binding are denoted by red asterisks.

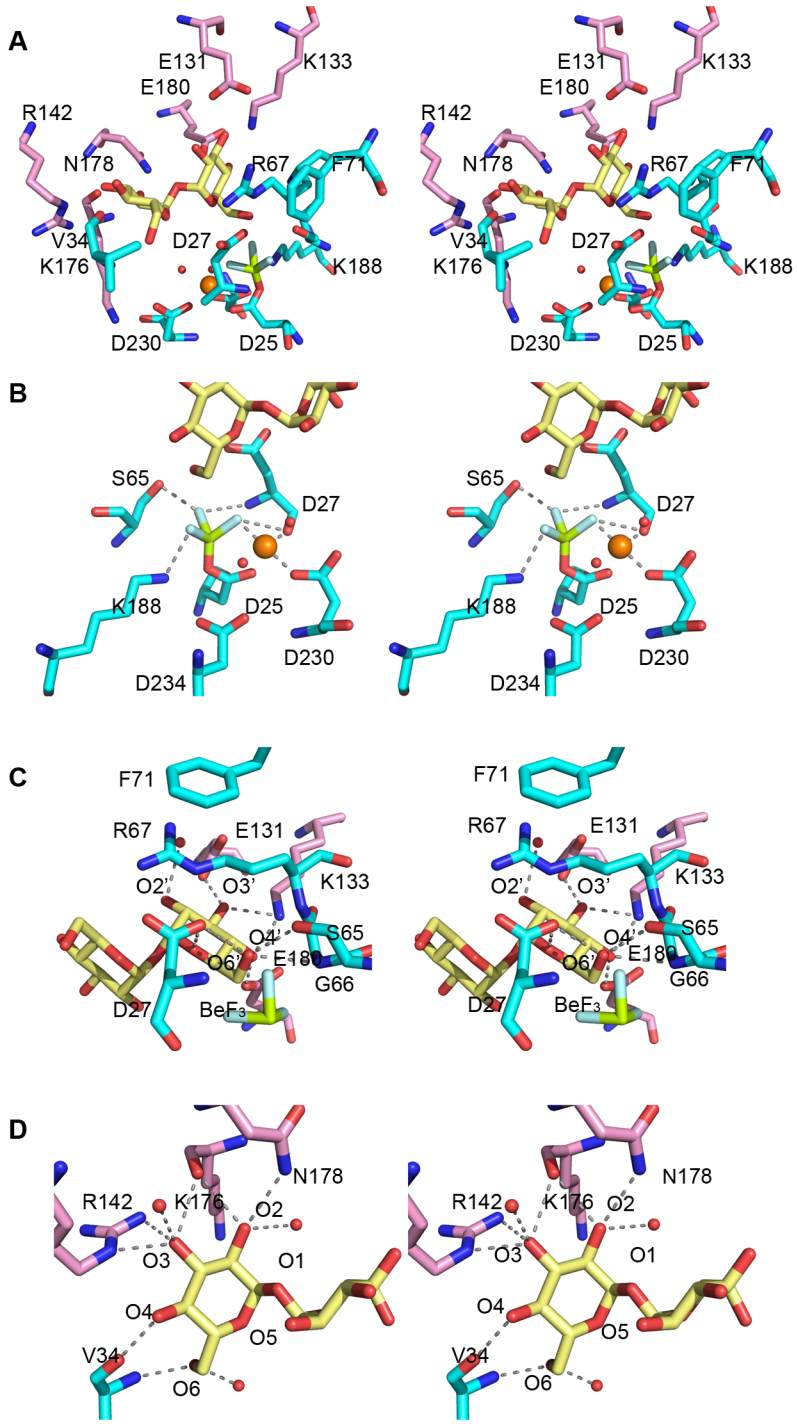

Figure S5. Stereoviews of the *C. albicans* Tps2PD catalytic pocket.

(A) Stereoview of the *C. albicans* Tps2PD-BeF_3-trehalose complex. **(B)** Walleye stereoviews of Tps2PD-BeF_3-trehalose complex showing the interactions between the protein and the F_3 covalently bound to residue D25. **(C)** Walleye stereoview of the interactions of Tps2PD residues with the one glucose moiety of trehalose. **(D)** Walleye

stereoview of the interactions of Tps2PD residues with the second glucose moiety of trehalose. Panels B through D correspond to panels C-E of Fig. 3 in the main text. Cap-domain residues are colored pink and core-domain residues are colored cyan. Trehalose is colored yellow. In each panel interactions are indicated by dashes. For the sake of clarity not all interactions are shown. See Figure Legend 3 for further details.

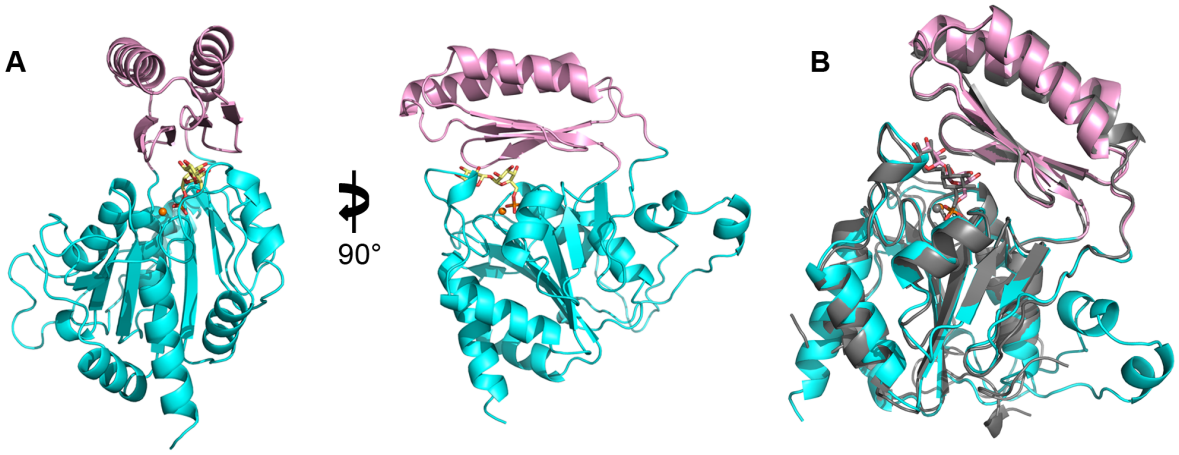

Figure S6. Structure of *C. neoformans* Tps2PD.

(**A**) Two views of the structure of the Tps2PD closed conformation structure. The core domains and cap domains are shown as cartoons and colored cyan and pink. T6P is shown as atom-colored yellow sticks and the Mg^{2+} ion is shown as an orange sphere. (**B**) Superposition of *C. albicans* Tps2PD and *C. neoformans* Tps2PD(D24N). *C. albicans* Tps2PD is shown in cartoon and colored grey.

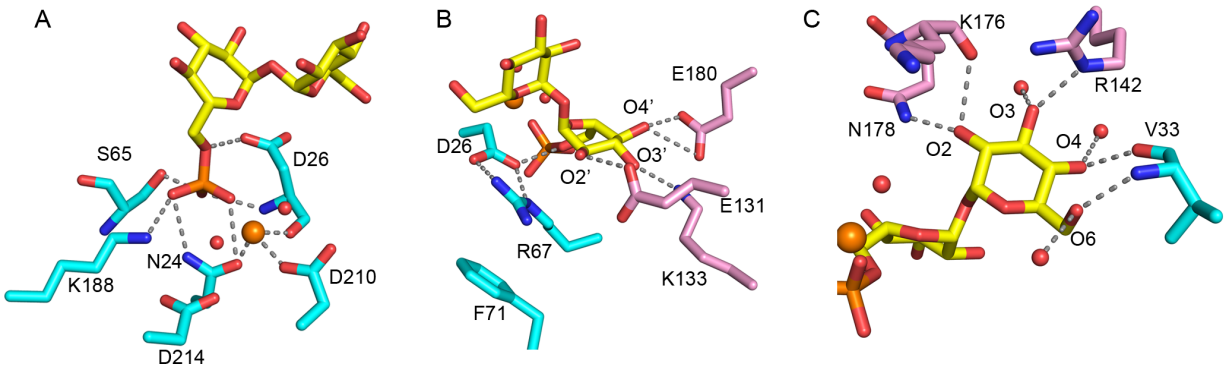

Figure S7. Active site of *C. neoformans* Tps2PD(D24N)-T6P complex.

(**A-C**) View of *C. neoformans* Tps2PD interactions with T6P. The cap-domain and core-domain residues are shown as atom-colored pink and cyan sticks and the magnesium ion and waters are depicted as spheres and colored orange and red, respectively. T6P is shown as atom-colored yellow sticks. Interactions between Tps2PD and T6P and the magnesium ion coordination are shown by dashes.

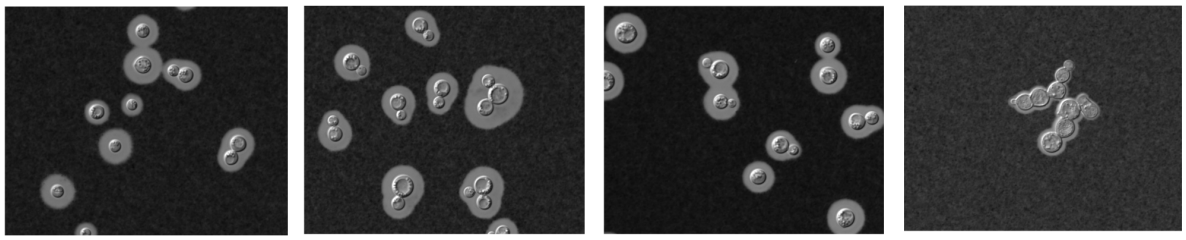

WT *tps2*Δ *tps2NTD*Δ *tps2D705N*

Figure S8. Loss of the Tps2 catalytic activity (D705N) impairs cell division and capsule production.

Cells were grown initially in YPD broth, washed, and resuspended in diluted Sabouraud (1/10) in MOPS buffer pH 7.3. Cells were grown overnight and stained with India ink. Large capsules were observed for all strains except for *tps2D705N*, which had a small capsule size and was defective in cell division. The *tps2NTD*Δ strain that retains the catalytic activity but has a deletion of the N-terminal domain had a phenotype similar to WT.

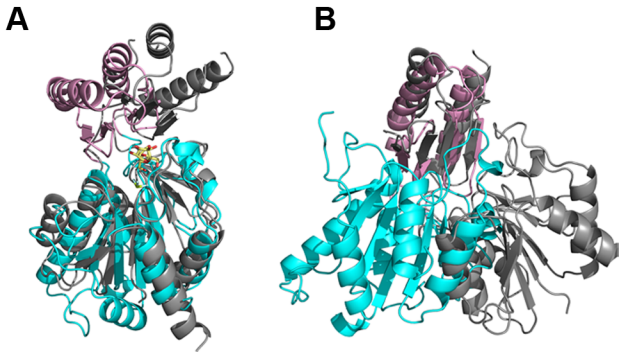

Figure S9. Superposition of *C. albicans* Tps2PD and *Brugia malayi* Tps2PD.

(**A**) Superposition of the core domains of *C. albicans* Tps2PD and *Brugia malayi* Tps2PD (residues 206-492). The *C. albicans* Tps2PD core domain and cap domain are shown as cartoons and colored in cyan and pink, respectively. The *Brugia malayi* Tps2PD is depicted as a grey colored cartoon. (**B**) Superposition of the cap domains of *C. abicans* Tps2PD and *Brugia malayi* Tps2PD (residues 206-492).

SI Appendix Tables

SI Appendix Table S1. Michaelis-Menten kinetics of *C. albicans* Tps2PD and variants

Construct	k_{cat} (s^{-1})	K_m (μM)	k_{cat}/K_m ($M^{-1}s^{-1}$)	Fold change
WT	36.8 ± 1.45	867.4 ± 69.7	4.2×10^4	1
D25N	ND[a]			
S65A	1.2 ± 0.06	3028 ± 205.5	0.4×10^3	105
R67A	ND			
E131A	1.1 ± 0.03	796.3 ± 58.7	1.4×10^3	30
K133A	0.27 ± 0.01	5414 ± 362.5	0.5×10^2	840
E180A	0.45 ± 0.004	101.8 ± 5.6	4.4×10^3	9.5
D230A	ND			

[a]ND represents no activity detected above detection limit.
± represents standard error.

Table S2. Data collection and refinement statistics for *C. albicans* Tps2

SI Appendix Table S2. Data Collection and Refinement Statistics for *C. albicans* Tps2[a]			
	C. albicans Tps2NTD	*C. albicans* Tps2PD-BeF_3-trehalose	*C. albicans* Se-Met Tps2PD-BeF_3-trehalose
Data Collection			
Space group	$P6_122$	$P2_12_12_1$	$P2_12_12_1$
Cell dimensions			
a, b, c (Å)	98.3, 98.3, 452.8	58.8, 87.2, 139.3	59.2, 87.2, 137.5
α, β, γ (°)	90, 90,120	90, 90, 90	90, 90, 90
Resolution (Å)	50.0-2.56 (2.60-2.56)	50.0-2.0 (2.03-2.0)	50.0-2.12 (2.16-2.12)
R_{merge} [b] (%)	9.8 (52.5)	5.3 (52.7)	8.0 (31.5)
I/σI	21.4 (2.5)	31.5 (2.8)	33.0 (5.7)
Completeness (%)	97.6 (92.2)	99.9 (100.0)	99.1 (93.8)
Redundancy	6.1 (5.5)	4.8 (4.7)	6.9 (5.7)
Overall figure of merit (FOM)			0.458
Refinement			
Resolution	48.9-2.56 (2.65-2.56)	36.4-2.0 (2.07-2.0)	-
No. reflections	42019	49177	-
R_{work} [c] /R_{free} [d] (%)	26.6/29.8	20.0/24.1	-
No. atoms			-
Protein	7451	4602	-
Ligand/ion	-	56	-
Water	98	395	-
B-factor			-
Protein	59.9	38.7	-
Ligand/ion	-	29.3	-
Water	47.5	42.8	-
RMS deviations			-
Bonds (Å)	0.006	0.008	-
Angles (°)	1.09	1.10	-
Ramachandran (%)			
Favored	94.7	97.4	-
Outlier	0.9	0	-

[a] statistics for the highest resolution shell are shown in parentheses.

[b] $R_{merge} = \Sigma|I - \langle I \rangle| / \Sigma|I|$, where I is the observed intensity and <I> is the average intensity of several symmetry-related observations.

[c] $R_{work} = \Sigma||F_o|-|F_c|| / \Sigma|F_o|$, where F_o and F_c are the observed and calculated structure factors, respectively.

[d] $R_{free} = \Sigma||F_o|-|F_c|| / \Sigma|F_o|$ for 5% of the data not used at any stage of the structural refinement.

Table S3. Data collection and refinement statistics for *C. neoformans* and *A. fumigatus* Tps2PD

SI Appendix Table S3. Data Collection and Refinement Statistics for *C. neoformans* and *A. fumigatus* Tps2PD[a]				
	C. neoformans Tps2PD(D24N)-T6P	*A. fumigatus* Tps2PD 1	*A. fumigatus* Tps2PD 2	*A. fumigatus* Tps2PD 3
Data Collection				
Space group	$P6_122$	$P22_12_1$	$P12_11$	$P12_11$
Cell dimensions				
a, b, c (Å)	63.1, 63.1, 284.3	45.4, 65.5, 118.5	39.8, 42.7, 80.2	45.0, 76.8, 83.7
α, β, γ (°)	90, 90,120	90, 90, 90	90, 99.5, 90	90, 94.4, 90
Resolution (Å)	50-2.15 (2.22-2.15)	50-1.57 (1.63-1.57)	50-1.65 (1.71-1.65)	50-1.89 (1.96-1.89)
R_{merge} [b]	0.088 (0.883)	0.108 (0.637)	0.077 (0.521)	0.07 (0.568)
I/σI	15.6 (2.7)	13.3 (3.5)	15.3 (3.6)	15.2 (2.7)
Completeness (%)	99.5 (99.8)	99.9 (99.0)	97.3 (89.0)	98.7 (84.8)
Redundancy	9.9 (9.6)	5.7 (5.6)	3.5 (2.2)	3.7 (3.5)
Overall figure of merit		0.537		
Refinement				
Resolution (Å)	43.3-2.15 (2.23-2.15)	36.0-1.57 (1.63-1.57)	20.6-1.65 (1.71-1.65)	31.8-1.89 (1.96-1.89)
No. reflections	19254	49835	31559	44688
R_{work} [c] / R_{free} [d] [%]	23.0/26.7	20.0/23.0	21.9/25.3	20.7/25.0
No. atoms				
Protein	2412	2257	2122	4344
Ligand/ion	32	-	1	2
Water	96	392	240	186
B-factor				
Protein	53.0	19.9	28.6	45.2
Ligand/ion	47.0	-	19.2	27.4
Water	49.6	29.7	38.4	48.0
RMS deviations				
Bonds [Å]	0.005	0.006	0.007	0.009
Angles [°]	0.71	1.01	1.05	1.15
Ramachandran (%)				
Favored	98.4	98.6	97.3	97.0
Outlier	0	0	0	0

[a] statistics for the highest resolution shell are shown in parentheses.

[b] $R_{merge} = \Sigma|I- \langle I\rangle|/ \Sigma|I|$, where I is the observed intensity and <I> is the average intensity of several symmetry-related observations.

[c] $R_{work} = \Sigma||F_o|-|F_c||/ \Sigma|F_o|$, where F_o and F_c are the observed and calculated structure factors, respectively.

[d] $R_{free} = \Sigma||F_o|-|F_c||/ \Sigma|F_o|$ for 5% of the data not used at any stage of the structural refinement.

SI Appendix References

1. Eschenfeldt WH, Stols L, Millard CS, Joachimiak A, & Donnelly MI (2009) A Family of LIC Vectors for High-Throughput Cloning and Purification of Proteins. *Methods in Molecular Biology,* Methods in Molecular Biology, ed Doyle SA), Vol 498, pp 105-115.

2. Massey SE*, et al.* (2003) Comparative evolutionary genomics unveils the molecular mechanism of reassignment of the CTG codon in *Candida* spp. *Genome Res.* 13(4):544-557.

3. Zheng L, Baumann U, & Reymond JL (2004) An efficient one-step site-directed and site-saturation mutagenesis protocol. *Nucleic Acids Res.* 32(14).

4. McCoy AJ*, et al.* (2007) Phaser crystallographic software. *J. Appl. Crystallogr.* 40:658-674.

5. Gibson RP, Tarling CA, Roberts S, Withers SG, & Davies GJ (2004) The donor subsite of trehalose-6-phosphate synthase - Binary complexes with UDP-glucose and UDP-2-deoxy-2-fluoro-glucose at 2 angstrom resolution. *J. Biol. Chem.* 279(3):1950-1955.

6. Terwilliger TC*, et al.* (2009) Decision-making in structure solution using Bayesian estimates of map quality: the PHENIX AutoSol wizard. *Acta Crystallogr. Sect. D-Biol. Crystallogr.* 65:582-601.

7. Emsley P & Cowtan K (2004) Coot: model-building tools for molecular graphics. *Acta Crystallogr. Sect. D-Biol. Crystallogr.* 60:2126-2132.

8. Otwinowski Z & Minor W (1997) Processing of X-ray diffraction data collected in oscillation mode. *Methods Enzymol.* 276:307-326.

9. Afonine PV*, et al.* (2012) Towards automated crystallographic structure refinement with phenix.refine. *Acta Crystallogr. Sect. D-Biol. Crystallogr.* 68:352-367.

10. Toffaletti DL, Rude TH, Johnston SA, Durack D, & Perfect J (1993) Gene transfer in *Cryptococcus neoformans* by use of biolistic delivery of DNA. *J. Bacteriol.* 175(5):1405-1411.

11. Zaragoza O & Casadevall A (2004) Experimental modulation of capsule size in *Cryptococcus neoformans*. *Biological procedures online* 6(1):10-15.